




Green biosynthetic silver nanoparticles from *Ageratum conyzoides* as multifunctional hemostatic agents: Combining hemostasis, antibacterial, and anti-inflammatory properties for effective wound healing

Yang Li^{a,1}, Yinfeng Tan^{a,1}, Huang Zhao^{a,1}, Shiting Chen^a, Azadeh Nilghaz^{b,c}, Rong Cao^{a,*}, Songlin Zhou^{a,**} 

^a NHC Key Laboratory of Tropical Disease Control, School of Tropical Medicine, Engineering Research Center of Tropical Medicine Innovation and Transformation of Ministry of Education, Hainan Provincial Key Laboratory of Research and Development on Tropical Herbs, Hainan Medical University, Haikou, Hainan, 571199, China

^b Drug Delivery, Disposition and Dynamics, Monash Institute of Pharmaceutical Sciences, Monash University, 381 Royal Parade, Parkville, Victoria, 3052, Australia

^c Institute for Frontier Materials, Deakin University, Waurn Ponds, Victoria, 3216, Australia

ARTICLE INFO

Keywords:

Silver nanoparticles
Ageratum conyzoides
 Hemostatic agent
 Biogenic synthesis
 Biocompatibility

ABSTRACT

Widespread interest in new hemostatic agents arises from the challenge of simultaneously satisfying the requirements of hemostatic, antibacterial, and anti-inflammatory properties while also considering the associated economic costs. An ideal hemostasis material should facilitate rapid hemostasis, intervene against infection, promote wound healing, and be cost-effective and easy to prepare. Herein, we demonstrate that medicinal plant-derived silver nanoparticles (AgNPs) exhibit the potential to constitute a promising multifunctional hemostatic reagent library. Biogenic synthesis of AgNPs utilizing *Ageratum conyzoides* extracts, referred to as AC-AgNPs, successfully combines the hemostatic and anti-inflammatory properties of *Ageratum conyzoides* with the inherent antibacterial activity exhibited by AgNPs. *In-vitro* coagulation experiments indicate that AC-AgNPs have a strong hemostatic effect, which is related to their size, concentration, and negative charge, and they exhibit low cytotoxicity and hemolysis. Subsequent experiments including scanning electron microscopy, flow cytometry, western blotting, and network pharmacology analysis have revealed that AC-AgNPs can cause platelet activation and aggregation, stimulated kallikrein-kinin system, shorten activated partial thromboplastin and prothrombin time, and increase fibrinogen content. These findings indicate that AC-AgNPs act on multiple signaling pathways, including endogenous and exogenous coagulation pathways, complement system, platelet activation, and aggregation. Furthermore, the hemostatic efficacy of AC-AgNPs is demonstrated in mouse models of tail amputation and liver injury, where AC-AgNPs significantly reduce the amount of blood loss and the bleeding time. Our work shows that AC-AgNPs possess strong hemostatic, anti-inflammatory, and antibacterial capabilities, ultimately facilitating wound healing. The biogenic synthesis of AgNPs from medicinal plants could be a multifunctional hemostatic candidate for practical application.

1. Introduction

Uncontrolled hemorrhage is a leading cause of preventable fatalities across battlefield scenarios and everyday settings such as outdoor activities, wilderness exploration, and traffic accidents [1]. Also, localized infection and inflammation at the wound site continue to be a challenging issue that could lead to delayed wound healing, amputation, or even death [2]. Early infection intervention and prompt and effective

hemostasis are thus important in reducing its economic and health consequences. Although there are already many commercial hemostatic products utilizing a diverse array of materials, such as aluminosilicate (for example, kaolin, montmorillonite, and zeolite), polysaccharide (including alginate, chitosan, and starch), and protein (including fibrin, gelatin, and thrombin), they are still far from perfect in terms of multifunctional implementation [3–5]. Therefore, developing advanced hemostatic materials with superior hemostatic, antibacterial, and

* Corresponding author.

** Corresponding author.

E-mail addresses: caorong_chem@163.com (R. Cao), zhousonglin106@163.com (S. Zhou).

¹ Y. Li, Y. Tan, and H. Zhao contributed equally to this work.

anti-inflammatory properties is valuable.

The past decade has witnessed a rapid increase in new hemostatic materials, among which nanotechnology-enabled materials exhibit unique advantages in hemorrhage management and related applications [6–8]. Some typical examples include a gold@halloysite nanotubes-chitin composite hydrogel with hemostatic and antibacterial activity [9], a 2-dimensional metal-organic framework nanosheet-loaded aerogel patch for wound management [10], and a peptide-modified hydrogel nanofibers with self-healing, antibacterial, and hemostatic properties [11]. Of these, silver nanoparticles (AgNPs) have attracted great interest due to their excellent antimicrobial activities, enabling a variety of biomedical uses, including wound dressings, disinfectant sprays, and surgical patches [12]. Several multi-purpose hemostatic materials have been synthesized by combining AgNPs with mesoporous silica granules, carboxyethyl chitosan-oxidized sodium alginate, and cyclodextrin metal-organic frameworks [13–15]. Although they have demonstrated the ability to execute multiple beneficial functions at wound sites, the imperfect performance concerning costs, safety, and preparation technology continues to drive innovative nanomaterial solutions. The facile addition of desirable functionalities into AgNPs could provide a more promising avenue for designing multifunctional hemostatic nanomaterials.

Regarding AgNP preparation, increasing efforts are being devoted to green synthesis utilizing biomolecules, microorganisms, and plant extracts [16,17]. Medicinal plant-mediated AgNP synthesis stands out as it provides a simple, eco-friendly, and economical fabrication strategy and confers biomedical benefits attributable to the phytochemical richness [18,19]. The medicinal plant components widely found in nature, with their unique chemical properties, serve as efficient reducing agents and stabilizers. Through a series of precise intermolecular interactions, these components undergo complexation with carefully designed nanoparticles. This process not only significantly enhances the structural stability of the nanoparticles but also ingeniously endows the resulting nanoparticles with a range of pharmacological properties, such as antitumor, antibacterial, antioxidant, alleviate diabetes mellitus, and anti-inflammatory effects, thereby broadening their application prospects in the biomedical field [20,21]. We noticed that herbal remedies boasting hemostatic qualities have been used for centuries and are still prevalent across regions globally. As such, it is anticipated that AgNPs derived from hemostatic herbal extracts possess the potential to not only halt bleeding but also exhibit other therapeutic properties.

Ageratum conyzoides L., a popular herb still used for medicinal purposes today, was selected to perform AgNP-mediated hemostatic therapy. *A. conyzoides* is widely distributed across tropical and subtropical regions worldwide, and its leaves and tender stalks are traditionally used as a remedy for bleeding, burns, eczema, headaches, and scalds [22]. A series of *A. conyzoides*-derived AgNPs (that is, AC-AgNPs) were successfully synthesized using aqueous herb extracts as green reducing and stabilizing agents. We previously reported the excellent anti-inflammatory properties performance of AC-AgNPs *in vitro* and *in vivo* [23]. Herein, we aim to take these green synthesized nanoparticles further by exploring the hemostatic effect of AC-AgNPs. The underlying coagulation mechanism of AC-AgNPs was successfully revealed through systematic evaluation of the *in vitro* and *in vivo* hemostatic efficacy of AC-AgNPs with varying particle sizes and surface charges. The wound dressing loaded with AC-AgNPs could accelerate the stoppage of bleeding by facilitating plasma aggregation and activating both internal and external hemostasis pathways. Benefiting from enriched medicinal phytoconstituents, AC-AgNPs displayed superior performance in hemorrhage management as well as antibacterial, anti-inflammatory effects. Moreover, biocompatibilities such as hemolysis, cytotoxicity, and skin irritation were evaluated. Our work presents a green synthesized AgNPs-mediated three-in-one hemostatic management solution that combines multifunctionality with cost-effectiveness in production.

2. Materials and methods

2.1. Synthesis and characterization of AgNPs

The aerial flower and leaf parts of *A. conyzoides* were gathered along the Meise River in Haikou City during the summer season of 2022. After thorough rinsing with milli-Q water, these parts were dried indoors under room temperature conditions and ground into a fine powder using a mortar and pestle. Subsequently, 1.0 g of this powder was dissolved in 60 mL of milli-Q water, subjected to an ultrasonic bath at 90 °C for 20 min, and allowed to cool. The resulting mixture was centrifuged at 12,000 g for 10 min, yielding a clear supernatant solution, constituting the aqueous extract of *A. conyzoides* (ACE). This fresh solution was then utilized for the biosynthesis of AC-AgNPs or freeze-dried to obtain ACE powder.

AC-AgNPs were synthesized by mixing and rotating different concentrations of ACE solution with AgNO₃ under varying time and temperature conditions. The solution was centrifuged at 4000 g for 0.5 h, and the obtained residue was washed with milli-Q water twice before being freeze-dried using a vacuum freeze dryer to obtain AC-AgNPs powder. Detailed synthesis parameters, conditions, and results are listed in Table S1.

Chemically synthesized AgNPs were obtained at room temperature by rotating 1 mM of AgNO₃ with 10 mM glucose for 2 h. The solution was centrifuged at 4000 rpm for 0.5 h and then freeze-dried using a vacuum freeze dryer to obtain AgNP powder.

We utilized an ultraviolet–visible (UV) spectrometer to verify the successful synthesis of AC-AgNPs or AgNPs. A dynamic light scattering (DLS) particle analyzer was used to determine the average particle size and charge of the synthesized AC-AgNPs or AgNPs. Transmission electron microscopy (TEM) was employed to observe the morphological characteristics of AC-AgNPs. Furthermore, ultra-performance liquid chromatography–quadrupole time-of-flight mass spectrometry (UPLC Q-TOF/MS) was adopted to analyze the chemical composition of the surface coating of AC-AgNPs.

2.2. Whole blood clotting time assay

The coagulation ability of various sizes and charges of AC-AgNPs was assessed. All subsequent procedures were carried out at 37 °C in Eppendorf tubes. After preheating, 1 mg of kaolin, or 8 µg of ACE, AgNPs, and different sizes and charges of AC-AgNPs, or 0, 2, 4, 8, or 16 µg of 55 nm, ζ –38 mV AC-AgNPs, was added to 1 mL of sodium-citrate pig blood. The test tubes were then incubated for 5 min at 37 °C in a water bath. To start the coagulation process, tubes were filled with a 1:10 vol ratio of recalcification reagent (0.2 M CaCl₂). The clotting process was monitored by shaking and tilting the tubes every 10 s. The clotting time was noted as the time until the blood had fully coagulated.

2.3. Analysis of the hemolytic properties of AC-AgNPs

To investigate the hemolyzed effect of AC-AgNPs on red blood cells (RBCs), 10 mL of pig blood (containing 0.35 % sodium citrate) was centrifuged at 150×g for 10 min at room temperature. The RBCs were obtained and washed three times with PBS, then diluted in PBS (1:20), plated in 96-well plates, and co-incubated for 12 h with different amounts of AC-AgNPs or AgNPs. Hemolysis was detected by evaluating hemoglobin levels. A microplate reader was employed to measure hemoglobin absorbance at 540 nm. The data was reported as a percentage of hemoglobin release, with 0.1 % Triton X-100 serving as a positive control and PBS as a negative control.

2.4. Cell culture and cytotoxicity

The human microvascular endothelial cell line (HMEC-1) was obtained from the ATCC (CRL-3243). HMEC-1 cells were cultured in an

MCDB131 medium with 100 U/mL penicillin and 100 µg/mL streptomycin in a humidified atmosphere containing 5 % CO₂ at 37 °C. Cells were passaged with trypsin-EDTA when they reached confluence and then subcultured into a new cell culture flask. Every second day, the medium was changed. The cytotoxicity of the AC-AgNPs on HMEC-1 cells was measured using a CCK8 assay kit following the manufacturer's instructions.

2.5. *In-vitro* KKS activation experiment

The freshly whole blood was collected from Sprague-Dawley (SD) rats, and 3.5 % sodium citrate was used as the anticoagulant at a volume ratio of 1:9. The plasma was obtained by centrifuging at 3000×g for 15 min at 4 °C. Then the plasma was treated with different concentrations of ζ -38 mV 55 nm AC-AgNPs (4 and 8 µg/mL), ζ -8 mV 59 nm AC-AgNPs (4 and 8 µg/mL), and ACE (4 and 8 µg/mL), respectively, at 37 °C for 2 h. The negative and positive controls were prepared using PBS and 1 mg/mL kaolin. After incubation, the above samples were subsequently submitted to Western blot for characterizing the cascade activation of the KKS system, including the cleavages of PPK (75 kDa), PK (52 kDa), FXII (80 kDa), and FXIIα (50 kDa), according to the protocol reported previously [24]. The primary antibodies used included anti-PPK (1:1000, Abcam, No. ab313891) and anti-FXII (1:1000, Abcam, No. ab242123), and the corresponding second antibodies were from Solarbio (1:500, Beijing, China). The development reagent was obtained from Pierce ECL (Boster, China).

2.6. Clinical standard blood coagulation assay

An automatic blood biochemical analyzer was used to measure clinically activated partial thromboplastin time (APTT), prothrombin time (PT), thrombin time (TT), and fibrinogen (FIB) levels. The fresh blood (containing 0.35 % sodium citrate) was centrifuged at 4000×g for 20 min to obtain the platelet-poor plasma (PPP). 500 µL of PPP was treated for 5 min at 37 °C with ζ -38 mV 55 nm AC-AgNPs (final concentration: 4 or 8 µg/mL) or kaolin (final concentration: 1 mg/mL) and assessed with an automatic coagulation analyzer.

2.7. Platelet activation analysis

Fresh whole blood was separated (1000 g, 10 min) at room temperature to prepare platelet-rich plasma (PRP). To limit the interference of plasma proteins, PRP was diluted in platelet diluent (1:10) and incubated at 37 °C. The diluent PRP and AC-AgNPs (final concentration: 8 µg/mL) were mixed and incubated in tubes at 37 °C for 20 min, then fixed for 30 min with 4 % paraformaldehyde. The mixture was then put on a glass slide and rinsed three times with PBS. Secondary cell fixation was performed with glutaraldehyde (2.5 %) and rinsed with PBS. The samples were vacuum-dried after being dehydrated in an ethanol series. The samples were examined using a field emission scanning electron microscope (FE-SEM) after sputtering with a thin layer of gold.

The flow cytometry (FCM) assay was then employed to quantify the platelet activation. 100 µL of whole blood was mixed with the test sample (final concentration, AC-AgNPs: 8 µg/mL, collagen: 1 mM, tirifiban (TIR): 10 µg/mL) for 5 min. Collagen was a positive control, while TIR was a selective and reversible platelet integrin receptor (Gp IIb/IIIa) antagonist in the operating experiment. Next, the treated blood was stained with platelet activation-dependent monoclonal antibodies (phycoerythrin (PE) anti-rat CD62p and fluorescein isothiocyanate (FITC) anti-rat CD41 were used as markers for platelet activation). Finally, the data was analyzed using a flow cytometer and FlowJo™ software (BD Biosciences).

2.8. Network pharmacology analysis

Initially, the potential targets for six active constituents of AC-AgNPs

were selected from SwissTarget Prediction (<http://www.swiss-targetprediction.ch>) databases, and target proteins of hemophilia were selected from GeneCards (<https://genecards.weizmann.ac.il/v3>) databases based on a relevance score ≥10. Then, a Venn diagram was created to identify the genes that overlapped between AC-AgNPs and hemophilia and to predict the overlapped genes that were considered the hemostatic targets of AC-AgNPs. Subsequently, these overlapped genes were imported into the STRING (www.string-db.org) platform to construct the protein-protein interaction (PPI) network. The protein type was set as "Homo sapiens". The free nodes were removed from the network, and the minimum required interaction score was set at a high confidence level of 0.700 to get the PPI data. After that, the data was imported into Cytoscape 3.9.1 software to calculate the degree of centrality, closeness centrality, and betweenness centrality of target genes, and then the core targets were screened. The blood clotting-related pathways were revealed by the metaspape (<https://metaspape.org>) platform based on Gene Ontology (GO) functional and KEGG pathway enrichment analyses. Finally, AutoDock Vina calculated the binding affinity and conformation of active ingredients and core targets (version 1.2.2) following the procedure described previously. They visualized the combinations with the lowest binding energies using PyMOL software and created two-dimensional schematic diagrams with Discovery Studio software.

2.9. *In-vivo* experiments

2.9.1. Animals

Pathogen-free C57BL/6 mice (male, 6–8 weeks old, ~20 g) and Sprague-Dawley (SD) rats (6–8 weeks, 200–250 g) were purchased from TianQing Animal Technology Company (Changsha, China) for *in vivo* animal studies. All procedures on animals follow guidelines established by the Institutional Animal Care Committee and the China Council on Animal Care at Hainan Medicine University (Grant HYLL-2022–028). All *in vivo* treatments were performed on three independent mice unless otherwise specified.

2.9.2. Tail amputation experiment

The *in-vivo* hemostatic properties of AC-AgNPs were first evaluated using the mouse-tail amputation model. C57BL/6 mice received caudal vein injection with AC-AgNPs (1 or 5 mg/kg) or protamine sulfate (PS, 5 mg/kg) once a day for 2 h before injection of 3 % sodium pentobarbital (40 mg/kg). The mouse, 1 cm away from the tip of the tail, was cut with surgical scissors, and then the tail was dipped with a prepared cotton ball every 15 s until the tail stopped bleeding. The blood loss and hemostasis time were recorded.

2.9.3. Liver injury experiment

The C57BL/6 mice were anesthetized, and the left abdomen was opened to expose the liver. After the liver surface was pierced with 18 G acupuncture, the wound was covered with gauze, commercial gelatin, and a hemostatic cotton ball containing AC-AgNPs (the cotton ball was immersed in 1 mg/mL of AC-AgNPs solution and then obtained by freeze-drying) and the bleeding was stopped with gentle pressure. The bleeding status was recorded every 10 s until the bleeding was stopped entirely, and the time and amount of bleeding were recorded. The blank group was not pressed; only a hemostatic cotton ball was used to absorb the blood on it. The gauze was used as the control group. Each group was randomly selected for testing, and the experimental results were averaged.

2.9.4. Coagulation factors were measured *in vivo*

The SD rats were administered AC-AgNPs (1 or 5 mg/kg), protamine sulfate (PS, 5 mg/kg), or normal saline by caudal vein injection. After 2 h, the control group was injected with normal saline, and all the other groups were injected with a heparin sodium injection (500 U/kg). Then, 30 min later, the rats were anesthetized with 3 % sodium pentobarbital

(40 mg/kg). 5 mL of blood was collected from the abdominal aorta *via* a negative vacuum pressure tube containing sodium citrate (1:9), followed by centrifugation at $4000\times g$ for 20 min to obtain plasma, and their corresponding ELISA kits measured the 6-keto-PGF1a, TXB2, tPA, and PAI-1 of plasma; the automatic blood biochemical analyzer detected the APTT, PT, TT, and FIB. 2 mL of blood was collected by a negative vacuum pressure pipe containing EDTAK2 to detect whole blood viscosity (WBV) and plasma viscosity (PV), and 1.6 mL of blood was collected with a negative pressure vacuum tube containing sodium citrate (1:4) to determine erythrocyte sedimentation rate (ESR) and hematocrit (HCT).

2.9.5. *In vivo* wound healing test

The C57BL/6 mice were randomly divided into three groups; each group contained five mice. The mice were acclimatized for one week before surgery. Mice were anesthetized with 3 % sodium pentobarbital and shaved, and then full-thickness wounds with a diameter of 6 mm were made on the dorsal skin using a biopsy punch. One group was dressed in gauze as negative controls, one group was dressed in gelatin as positive controls, and one group was dressed in hemostatic gauze containing AC-AgNPs (the gauze was immersed in 1 mg/mL of AC-AgNPs solution and then obtained by freeze-drying). Every day, the wound area was monitored, and the area was measured by Image J software. Wound regeneration (%) was calculated using the equation:

$$\text{Wound contraction} = (\text{area (0 days)} - \text{area (n day)}) / \text{area (0 days)} \times 100\%$$

2.10. Statistical analysis

The experimental data were analyzed using a Student's t-test. *P* values of less than 0.05 were considered statistical significance. Results

are expressed as mean \pm standard error (s.e.m.) for animal studies, while the other results are expressed as mean \pm standard deviation (s.d.).

3. Results and discussion

3.1. Design and synthesis of AC-AgNPs

Since green synthesis can effectively combine the inherent antibacterial activities of AgNPs with the therapeutic properties of medicinal plants [25–27], the resulting AgNPs may emerge as potential candidates for hemostatic applications. To this end, *A. conyzoides*, a traditional hemostatic herb, synthesized AgNPs. As depicted in Fig. 1A, Fig. S1, and Table S1, size- and surface-charge-controlled AC-AgNPs were fabricated *via* an eco-friendly one-pot phytosynthesis technique. In our previous work, based on the chemical equation $3\text{Ag} + 4\text{HNO}_3 = 3\text{AgNO}_3 + \text{NO} + \text{H}_2\text{O}$ (1) and $\text{AgNO}_3 + \text{NaCl} = \text{AgCl} + \text{NaNO}_3$ (2), we calculated that elemental silver accounted for about $32.71 \pm 4.87\%$ of the synthesized AC-AgNPs [23]. UHPLC-ESI-Q-TOF-MS analysis of the phytochemical profile of AC-AgNPs revealed a surface enrichment of five flavonoids and a polyhydroxycyclohexanoic acid (Fig. S2), which tend to form a corona on the nanoparticle surface in a hydrated environment [23]. These phytoconstituents have rich hydroxyl and carboxyl groups, and their dissociation contributes to the negative charging of the AgNP surface. In our preliminary study, AC-AgNPs were proven to have superior anti-inflammatory effects *in vitro* and *in vivo* due to their capping with plant extracts [28]. Furthermore, to ensure reproducibility in green AC-AgNP synthesis, we strictly standardize our methods, controlling plant species, growth conditions, and extraction to maintain phytochemical uniformity. We also closely monitor reaction parameters, ensuring consistent AC-AgNP properties across batches. While natural variability exists, our controlled processes yield AC-AgNPs with good repeatability, a key aspect of green synthesis.

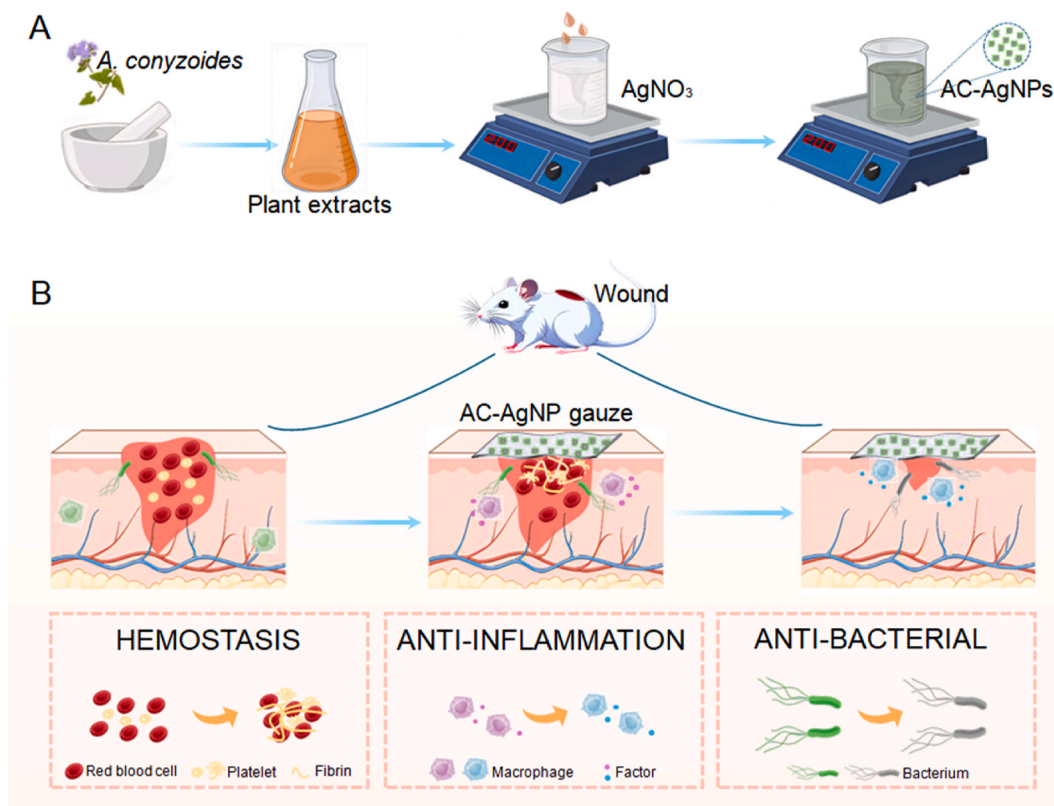


Fig. 1. (A) Schematic illustration of the biogenic synthesis of AC-AgNPs. (B) AC-AgNPs exhibit a three-in-one combination of hemostatic, anti-inflammatory, and antibacterial properties.

To explore the potential of AC-AgNPs as hemostatic materials, herein we further evaluated their hemostatic and antibacterial activities (Fig. 1B). Specifically, we investigated the hemostatic efficacy and mechanism of AC-AgNPs with varying sizes and charges using *in-vitro* and *in-vivo* models. Also, we assessed the antibacterial activity of AC-AgNPs against *Escherichia coli*, *Klebsiella pneumoniae*, *Pseudomonas aeruginosa*, and *Staphylococcus aureus*.

3.2. *In-vitro* blood clotting performance of AC-AgNPs

To evaluate the hemostatic potential of AC-AgNPs, an *in vitro* whole-blood clotting test was first performed. As expected, AC-AgNPs with a zeta potential of about -15 mV exhibited outstanding coagulation performance at a concentration of $8 \mu\text{g/mL}$ (Fig. 2A). When compared to the negative control (PBS), the coagulation efficiency of AC-AgNPs was dramatically increased by nearly 3 times. Increasing particle size from 30 nm to 120 nm only slightly increases the coagulation effect. Also, as evidenced by the similar coagulation time, the blood clotting performance of these AC-AgNPs *in vitro* is comparable to that of kaolin, which has orders of magnitude higher concentration and is a popular commercial hemostatic agent. By contrast, the chemically synthesized AgNPs with similar size and negative charge show no significant effect on coagulation, even at $100 \mu\text{g/mL}$ concentrations. Surface coating can profoundly affect the hemostatic performance of AgNPs. As shown in Fig. 2A, aqueous extracts of the aboveground part of *A. conyzoides* could accelerate blood coagulation and reduce the clotting time at $8 \mu\text{g/mL}$. The capping enriched with bioactive molecules from ACE endows AC-AgNPs with excellent procoagulant potential. We then examined the

effects of the charge and concentration of AC-AgNPs on the coagulation ability. It was found that the blood clotting ability strongly relies on both particle surface charge and concentration. As shown in Fig. 2B, AC-AgNPs with a more negative surface charge could provide higher coagulation efficiency within a similar particle size range. More specially, the clotting time gradually decreased from 310 to 170 s as the zeta potential increased from -8 mV to -38 mV. The particle concentration also has a significant impact on blood clotting performance. A threefold decrease in coagulation time was observed when the particle concentration increased from 2 to $8 \mu\text{g/mL}$ (Fig. 2C). As the concentration continued to increase, the clotting time no longer changed significantly, showing a 4-fold decrease relative to the PBS controls. In addition, the biocompatibility of AC-AgNPs was evaluated using *in vitro* cytotoxicity and hemolysis assays. As shown in Fig. 2D, during 24 h incubation, the growth of HMEC-1 cells could be suppressed until the particle concentration increased to $32 \mu\text{g/mL}$, and its cell viability decreased to 85% ($P < 0.05$). In comparison, the chemically synthesized AgNPs with a concentration of $16 \mu\text{g/mL}$ showed considerable inhibition effect on cell growth. The green synthesis of AgNPs can reduce their cytotoxic and oxidative effects due to their capping with biologically compatible and boosting molecules such as flavonoids, which is consistent with the previous reports [29,30]. Similarly, the hemolytic performance of AC-AgNPs significantly depends on their concentration. The hemolysis test was conducted by spectrophotometric measurement of hemoglobin release after exposure to various doses of AC-AgNPs, using Triton X-100 as the positive control and PBS as the negative control. No significant hemolysis was detected at concentrations of AC-AgNPs below $32 \mu\text{g/mL}$. At the same time, the chemically

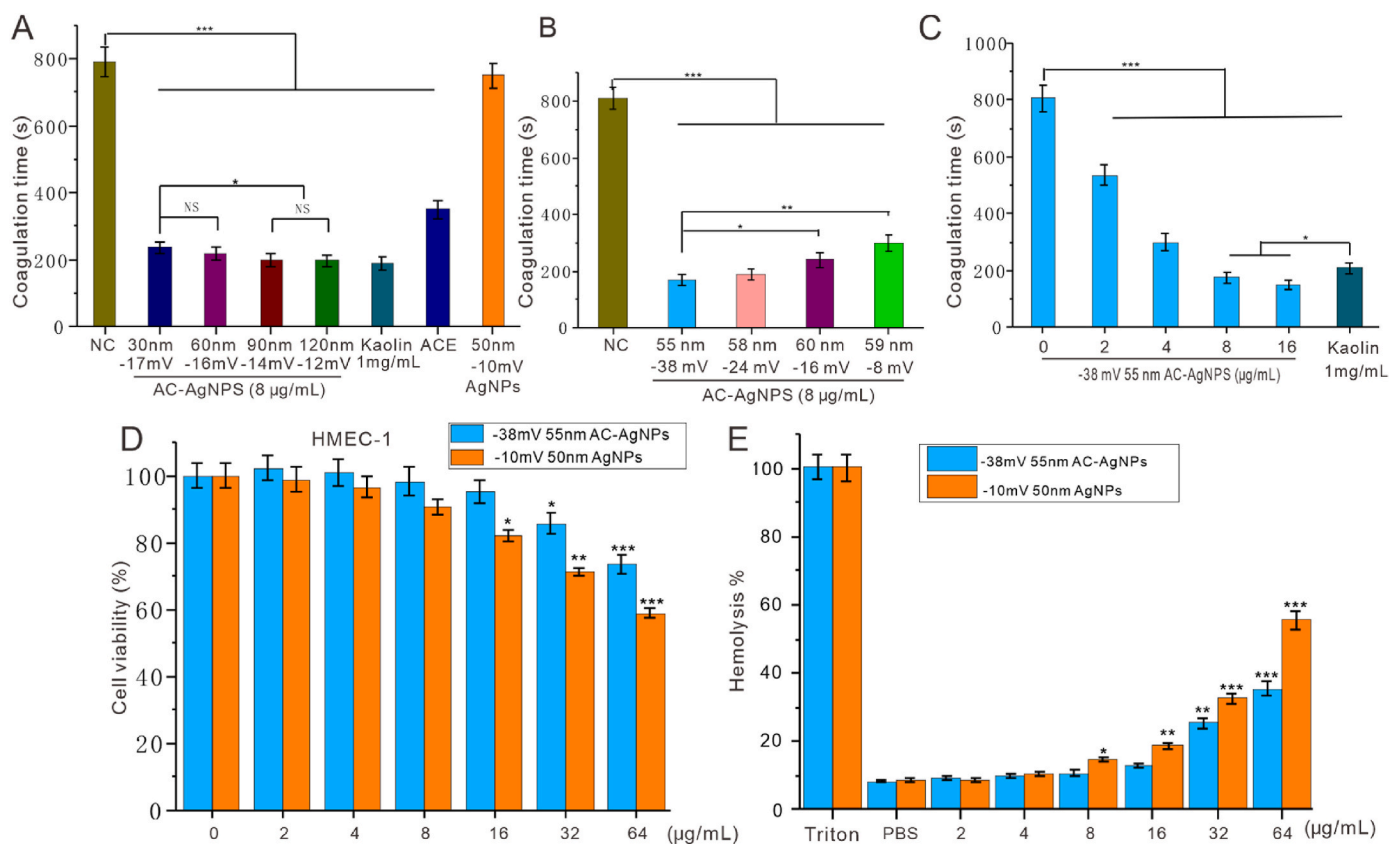


Fig. 2. *In-vitro* blood-clotting performances of AC-AgNPs. (A) Coagulation time of AC-AgNPs at $8 \mu\text{g/mL}$ with various particle sizes, chemically synthesized AgNPs ($8 \mu\text{g/mL}$), and ACE ($8 \mu\text{g/mL}$). The negative and positive controls were PBS and kaolin (1 mg/mL). (B) Coagulation time of AC-AgNPs with various negative charges. (C) Coagulation time of AC-AgNPs (-38 mV, 55 nm) with various concentrations. (D) Cytotoxicity analysis of AC-AgNPs (-38 mV, 55 nm) and chemically synthesized AgNPs (-10 mV, 50 nm). (E) Hemolysis analysis of AC-AgNPs (-38 mV, 55 nm) and AgNPs (-10 mV, 50 nm). PBS and Triton X-100 (0.1%) were negative and positive controls, respectively. Statistical significance was determined versus the negative controls (NC) group (one-way ANOVA followed by a Student's t-test). * $P < 0.05$, ** $P < 0.01$, *** $P < 0.001$.

synthesized AgNPs exhibited observational hemolytic activities at concentrations as low as 8 $\mu\text{g}/\text{mL}$ (Fig. 2E). These results indicated that AC-AgNPs could provide sufficient hemocompatibility and cytocompatibility up to a maximum concentration of 16 $\mu\text{g}/\text{mL}$.

3.3. Coagulation pathway and platelet activation of AC-AgNPs

To clarify the hemostatic mechanism of AC-AgNPs, coagulation tests, including APTT, PT, TT, and FIB, were first performed. As shown in Fig. 3A, AC-AgNPs *in vitro* activated the intrinsic pathway of coagulation as measured by APTT assays. AC-AgNPs at 8 $\mu\text{g}/\text{mL}$ could shorten the APTT by 70.5% (−8 mV) and 58.3% (−38 mV), respectively, relative to the negative control. AC-AgNPs (8 $\mu\text{g}/\text{mL}$, −38 mV) show slightly faster clotting performance than kaolin, with positive control at 1 mg/mL. Besides, the APTT value of ACE was reduced compared with PBS, suggesting that the phytochemicals could directly participate in the intrinsic pathway of the coagulation cascade reaction and enhance procoagulant activity. The APTT of AC-AgNPs at 8 $\mu\text{g}/\text{mL}$ with a zeta potential of −38 mV was lower than that of plant extracts, which might be attributed to the enrichment of hemostatic phytoconstituents on the negatively charged surface of AC-AgNPs. PT is an indicator of the activation of an extrinsic coagulation pathway. PT values of AC-AgNPs can be slightly lower than that of blank ($P < 0.05$). However, ACE at the 8 $\mu\text{g}/\text{mL}$ level could not activate the external coagulation pathway. Based on these observations, it is conceivable that AC-AgNPs, through enrichment, may enable plant metabolites to activate the external coagulation pathway to some extent (as discussed later). Furthermore, an increase in FIB concentration was observed for both AC-AgNPs and ACE groups, demonstrating that AC-AgNPs significantly affect plasma

coagulation time.

It is well-known that KKS cascade activation as a contact zymogen system in plasma plays a key role in hematological hemostasis [31]. Upon contact with negatively charged surfaces, the zymogen factor XII (FXII) undergoes autoactivation, leading to the formation of FXII α and subsequent activation of PPK, thereby contributing to the coagulation process [32]. To further uncover the underlying molecular mechanisms of the procoagulant activity of AC-AgNPs, the *in-vitro* activation of PPK and FXII in pig plasma was assessed using Western blot analysis. As shown in Fig. 3B–D, stimulating plasma samples with AC-AgNPs reduces the zymogen content of PPK and FXII while concomitantly enhancing the levels of their active forms, PK and FXII α , in a concentration- and charge-dependent manner. AC-AgNPs can accelerate thrombosis by activating the intrinsic coagulation cascade, which cross-talks with the KKS system *via* FXII activation and subsequent activation of FX α . However, the results in Fig. 3B–D also shows that ACE does not induce the cascade activation of KKS, suggesting that the clotting effect of plant extracts is achieved through other pathways. These results show that AC-AgNPs enhance the propagation of the intrinsic pathway *via* a classical mechanism strongly dependent on factor FXII, owing to the synergistic effect of surface negative charges and phytochemicals. When the concentration of AC-AgNPs reaches 8 $\mu\text{g}/\text{mL}$ and its zeta potential reaches −38 mV, it exhibits a higher ability to cleave the two proenzymes into active proteins compared to classical activators of the intrinsic coagulation pathway, such as kaolin.

In addition, previous studies have demonstrated that platelets and the coagulation cascade are activated simultaneously, with crosstalk occurring between these two pathways [32]. For instance, thrombin is a potent activator of human platelets *via* cleavage of protease-activated

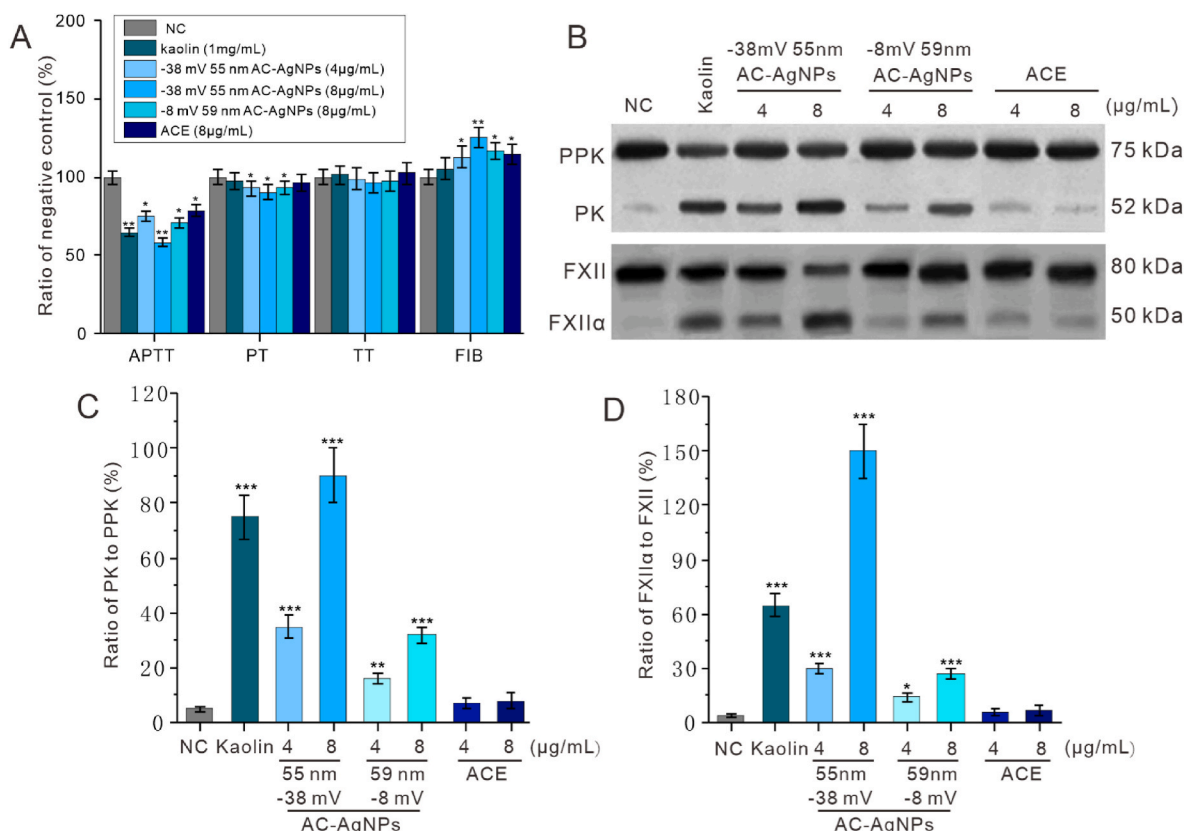


Fig. 3. Coagulation pathway and KKS cascade activation by AC-AgNPs. (A) Study of four coagulation indices (APTT, PT, TT, and FIB) on plasma treated with various AC-AgNPs and AC-Extract. PBS and kaolin (1 mg/mL) were negative and positive controls, respectively. (B) *In-vitro* assays for PPK and FXII cleavage and PK and FXII α formation in plasma induced by a series of concentrations of AC-AgNPs or AC-Extract. (C) Statistical results of the PK to PPK ratio. (D) Statistical results of the FXII α to FXII ratio. Statistical significance was determined versus the negative controls (NC) group (one-way ANOVA followed by Student's t-test). * $P < 0.05$, ** $P < 0.01$, *** $P < 0.001$.

receptors (PARs, specifically PAR1 and PAR4), while FIB acts as a bridge between activated platelets. In turn, activated platelets augment coagulation by supplying coagulation factors and presenting a negatively charged phospholipid surface, which promotes the assembly of cofactor/coagulation protease complexes and subsequent thrombin generation [33]. Then, we investigated the effect of AC-AgNPs on platelet activation. The SEM images show that platelets in the control group have a smooth surface and a scattered distribution of discoid-shaped platelets. At the same time, AC-AgNPs significantly induce platelet activation, as evidenced by pseudopodia formation, membrane budding, and aggregation (Fig. 4A). Typically, once platelet activation occurs, intracellularly distributed adhesion molecule CD62p migrates to the platelet membrane's surface, and its expression levels rise. To further investigate the effect of AC-AgNPs on platelet activation, freshly prepared plasma with rich platelets was incubated with AC-AgNPs at 8 $\mu\text{g}/\text{mL}$, and the platelets were analyzed by flow cytometry for expression of the activation marker CD62p. As shown in Fig. 4B, AC-AgNPs exhibited a marked ability to stimulate platelet activation, with a proportion of activated platelets reaching $42.8 \pm 3.8\%$. It signifies a 3.3-fold increase compared to the untreated control and achieves an effect of $\sim 80\%$ of the positive control (1 mM collagen). Meanwhile, we found that the AC-AgNPs can reverse tirofiban's (a GPIIb/IIIa inhibitor) inhibition of platelet activation. The proportion of activated platelets rose from $6.7 \pm 1.1\%$ to $10.9 \pm 1.9\%$, nearly close to the untreated control. These results suggest that AC-AgNPs may induce platelet activation and aggregation by the GPIIb/IIIa receptor pathway, which could trigger the hematological coagulation cascade.

3.4. Hemostatic mechanism of AC-AgNPs

To further explore the hemostatic mechanism of AC-AgNPs, we employed a network pharmacology approach to identify the target proteins in the coagulation system that are influenced by the six main phytoconstituents present on the surface of AC-AgNPs. We notice that hemophilia is a disease characterized by blocked blood coagulation due to a lack of coagulation factors [34,35]. Herein, we thus chose this disease, which is closely related to coagulation, as a breakthrough point to analyze the coagulation-related mechanisms of AC-AgNPs. As shown in Fig. 5A, by combining the GeneCards and DisGeNET databases, we screened out 463 potential therapeutic targets. Meanwhile, based on the SwissTarget Prediction database, we identified 206 target proteins as the potential activating components of these phytoconstituents. Among them, 23 overlapping targets were found via Venn diagram analysis. A constructed network map of "compound-hemophilia-common targets" using Cytoscape 3.9.1 software reveals that these six phytoconstituents can all act on multiple common target genes related to coagulation

(Fig. 5B). We then imported these 23 targets into the STRING platform to construct a protein-protein interaction (PPI) network diagram (Fig. 5C), which consists of 23 nodes and 83 edges, with an average Degree value of 7.4545, an average betweenness of 17.9091, and an average closeness of 0.0265. Of these, 13 core target proteins were selected with a degree value higher than the average as the core targets in the coagulation process (Table S2). Meanwhile, 23 overlapping targets were imported into the Metascape platform, where we identified 17 signaling pathways closely related to coagulation through GO and KEGG analysis, including blood clotting cascade, extrinsic pathway of fibrin clot formation, complement system, platelet activation, signaling and aggregation (Fig. 5D–Table S3, Figs. S3 and S4).

Subsequently, to evaluate the affinity between the compounds and the core target proteins, molecular docking was performed between 6 phytoconstituents as ligands and 13 core target proteins as receptors. The binding affinity below -7.0 kcal/mol indicates tight binding between the ligand and the receptor [36]. As shown in Fig. 5E, these compounds exhibit direct interactions with coagulation factors in the coagulation system (including F2, F3, F7, F9, F10, F11, and PROC), as well as with fibrinolytic system proteins (namely PLAT and PLG) and proteins related to platelet activation and inflammation (such as SELP, PTGS2, SRC, and KDR) [37–40]. Among them, amentoflavone-7,7'-dimethylether, 1,3,5-tricaffeoylquinic acid, and kaempferol 3,7,4'-triglycoside even exhibited superior binding affinities with multiple target proteins below -9.0 kcal/mol, indicating their key roles in the coagulation process. More specifically, amentoflavone-7,7'-dimethylether has binding affinities below -9.0 kcal/mol with seven proteins, including F2, F7, F9, F10, F11, PROC, PLAT, PTGS2, SRC, and KDR; 1,3,5-tricaffeoylquinic acid has binding affinities below -9.0 kcal/mol with four proteins, including F7, PLG, PTGS2, and SRC; kaempferol 3,7,4'-triglycoside has a binding affinity below -9.0 kcal/mol with the F11 protein. It is worth mentioning that the other three proteins (that is, kaempferol, ageconylflavone B, and 5,6,7,3',4',5'-hexamethoxy) also have binding affinities below -9.0 kcal/mol with the PTGS2 protein, thereby contributing to the coagulation process. Furthermore, PyMOL and LigPlus programs were used to analyze the docking conformation visually. As shown in Fig. 5F, the results indicate that all small-molecule ligands can bind tightly to the target protein, primarily through various forces, including hydrogen bonds, hydrophobic interactions, π -stacking, and salt bridges, maintaining a spacing of 2–4 Å. Notably, hydrophobic forces allow each small molecule compound to form hydrophobic interactions with 5–10 amino acids of the target protein, suggesting the structural basis for the resulting stable complexes. These findings indicate that key phytoconstituents on the surface of AC-AgNPs can potentially target various pathways, including the intrinsic coagulation pathway, extrinsic coagulation pathway, complement system, and

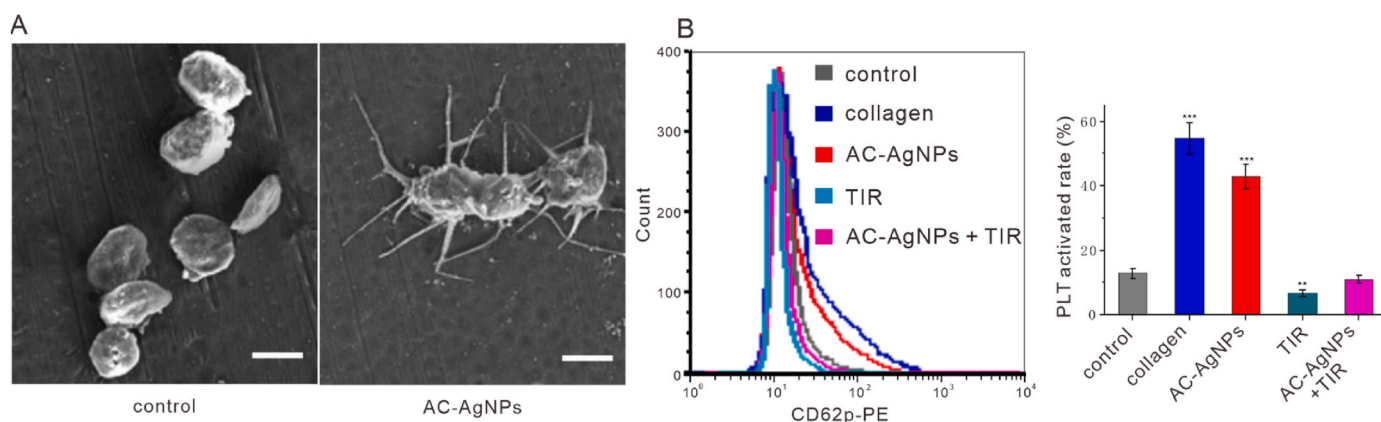


Fig. 4. Platelet activation induced by AC-AgNPs. (A) SEM images of resting and activated platelets. (B) FCM analysis of platelet activation (CD62p⁺) of AC-AgNPs. Fresh blood without treatment (control), collagen (positive control), and tirofiban (reversion) ($n = 3$). Statistical significance was determined versus the NC group (one-way ANOVA followed by a Student's *t*-test). ** $P < 0.01$, *** $P < 0.001$.

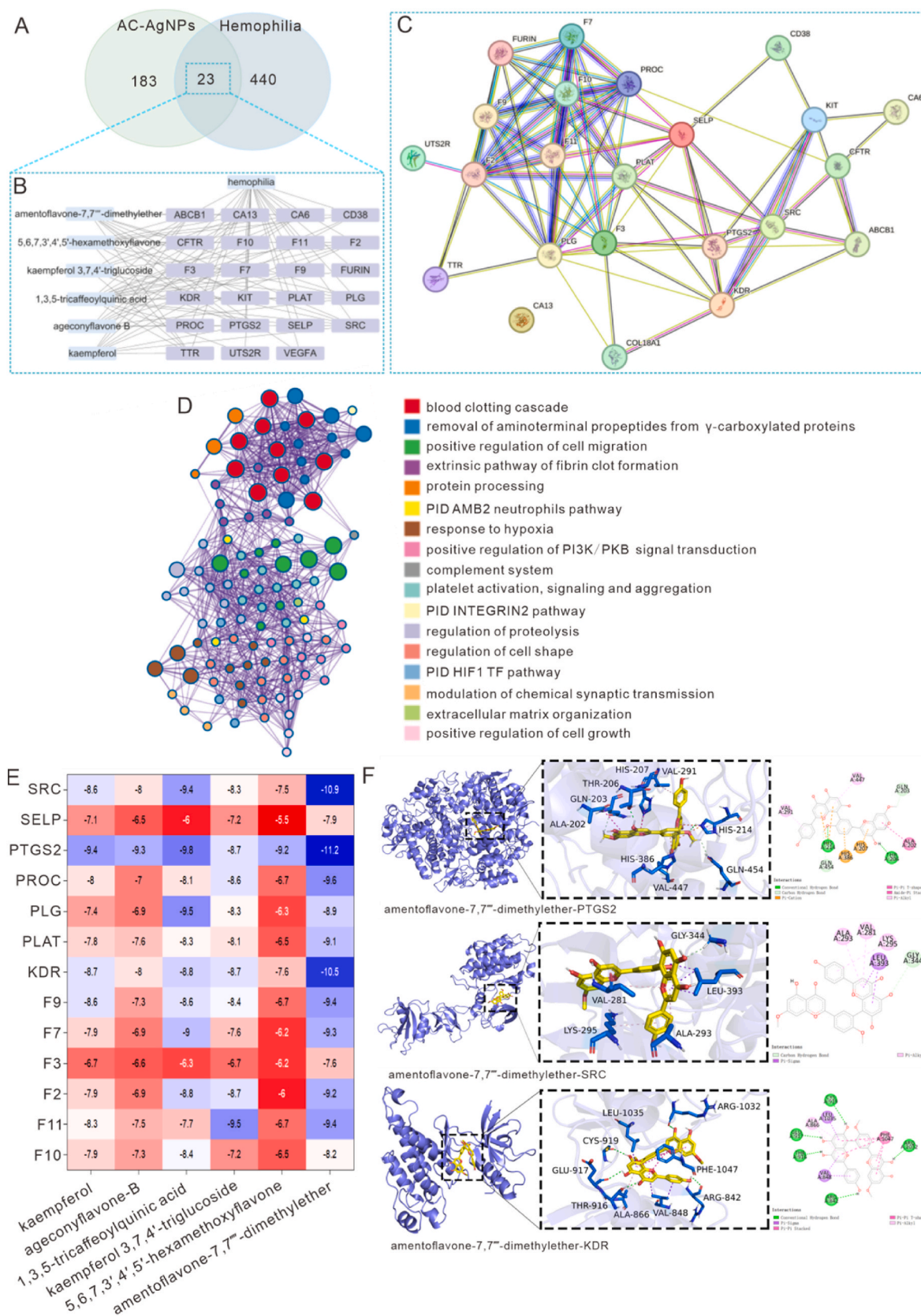


Fig. 5. Network pharmacology analysis of the hemostatic mechanism of AC-AgNPs. (A) The overlapped targets of AC-AgNPs and hemophilia are shown in the Venn diagram. (B) Network diagram of “compound-hemophilia-common targets”. (C) PPI network diagram of common targets. (D) A network of the enriched terms with a similarity >0.3 are connected, colored by cluster ID, where nodes that share the same cluster-ID are typically close to each other. (E) Heat map of the docking score between core targets and active compounds. (F) Visualization of amentoflavone-7,7'''-dimethylether interconnecting with the PTGS2, SRC, and KDR proteins.

platelet activation, thereby exerting a hemostatic effect.

3.5. In-vivo hemostatic efficacy of AC-AgNPs

AC-AgNPs were next investigated *in vivo* for the ability to halt acute bleeding in a mouse tail amputation model and a mouse liver injury model, which are well-established models for determining hemostatic capability [41]. Up to 5 mg/kg of AC-AgNPs was used because our previous acute toxicity experiment demonstrated that administering this dosage to mice did not result in any noticeable toxic or side effects on their liver and kidneys [23]. As shown in Fig. 6A–C, when the mouse tail bleeding occurs, the blank group displays a long hemostatic time (335 ± 30 s) and a significant blood loss (225 ± 25 mg). As a positive control, protamine sulfate (PS) alone significantly decreases bleeding time and volume. A similar trend in reducing bleeding time and blood loss was observed in the AC-AgNP group. At a dose of 5 mg/kg, AC-AgNPs significantly reduced bleeding time and volume by approximately 68.7 % and 64.4 %, respectively, compared to the blank group. When active bleeding wounds occurred in the liver (Fig. 6D–E, and Fig. S5), AC-AgNPs exhibited a similar hemostatic performance. Bleeding stopped at 185 ± 20 s in the blank group but at 125 ± 15 s in the gauze-treated group and at 70 ± 10 s in the gelatin-treated group. Treatment with AC-AgNPs further reduced the bleeding time to 65 ± 10 s, resulting in the least blood loss of 68 ± 9 mg among all groups. The results from both *in-vivo* bleeding models indicate that AC-AgNPs have superior hemostatic efficacy and a fast procoagulant capability.

A rat model with heparin-induced anticoagulation was used to explore further the effect of AC-AgNPs on the clotting cascade *in vivo*. Heparin was chosen because it can bind to and enhance the inhibitory activity of the plasma protein antithrombin against some important serine proteases in the coagulation system [42]. PS, as an antiheparin agent that can neutralize the anticoagulant action of heparin, was utilized to develop a positive control group [43]. As shown in Fig. 7A–C, APTT and PT were significantly prolonged, and FIB concentration was reduced in the model group, indicating the successful establishment of

the model. A remarkable shortening of APTT and PT was observed in the positive control group. Similarly, the AC-AgNPs group demonstrated a significant reduction in coagulation time, indicated by the decrease in APTT and PT, when the concentration of AC-AgNPs reached 5 mg/kg. Moreover, an increase in FIB levels was observed in both the AC-AgNPs (1 and 5 mg/kg) groups, whereas the PS group did not show any obvious changes compared to the model group. These results, again, indicate that AC-AgNPs possess coagulant activity and contribute to achieving rapid hemostasis in the rat model.

In addition, thromboxane (TXA₂) and prostacyclin (PGI₂), as representative metabolites of arachidonic acid, regulate platelet activation, aggregation, and vasoconstriction, making them valuable indicators for assessing hemostatic effects [44]. Due to their instability, the corresponding stable metabolic products in the blood, TXB₂ and 6-keto-PGF₁α, are typically measured as indirect indicators of the content of TXA₂ and PGI₂, respectively [44]. Upon heparinization *in vivo*, the level of TXB₂ decreased by 29.6 %, while the level of 6-keto-PGF₁α increased by 31.4 % compared to the control group (Fig. 7D and E). A significant reversal trend was observed in the AC-AgNPs groups, with an increased level of TXB₂ and a decreased level of 6-keto-PGF₁α. However, PS could reverse the reduced level of TXB₂ but could not reverse the increased level of 6-keto-PGF₁α. Besides, tissue-type plasminogen activator (tPA) and plasminogen activator inhibitor-1 (PAI-1) were measured as two important regulatory factors of the blood fibrinolytic system [45]. As shown in Fig. 7F and G, there was a 51.3 % reduction in PAI-1 and a 112.1 % increase in tPA observed in the heparinized rats. The use of AC-AgNPs or PS could significantly inhibit both of these effects. Hemorheology, which is related to blood flow and pressure, flow volume, and blood vessel resistance, including whole blood viscosity (WBV), plasma viscosity (PV), packed cell volume (PCV), and erythrocyte sedimentation rate (ESR), is used to diagnose plasma viscosity problems in clinical settings [46]. Herein, we evaluated the impact of AC-AgNPs on the hemorheology of rats. As illustrated in Fig. 7H–K, following heparin treatment, these hemorheology indices, including WBV, PV, PCV, and ESR, were significantly lower in the model group

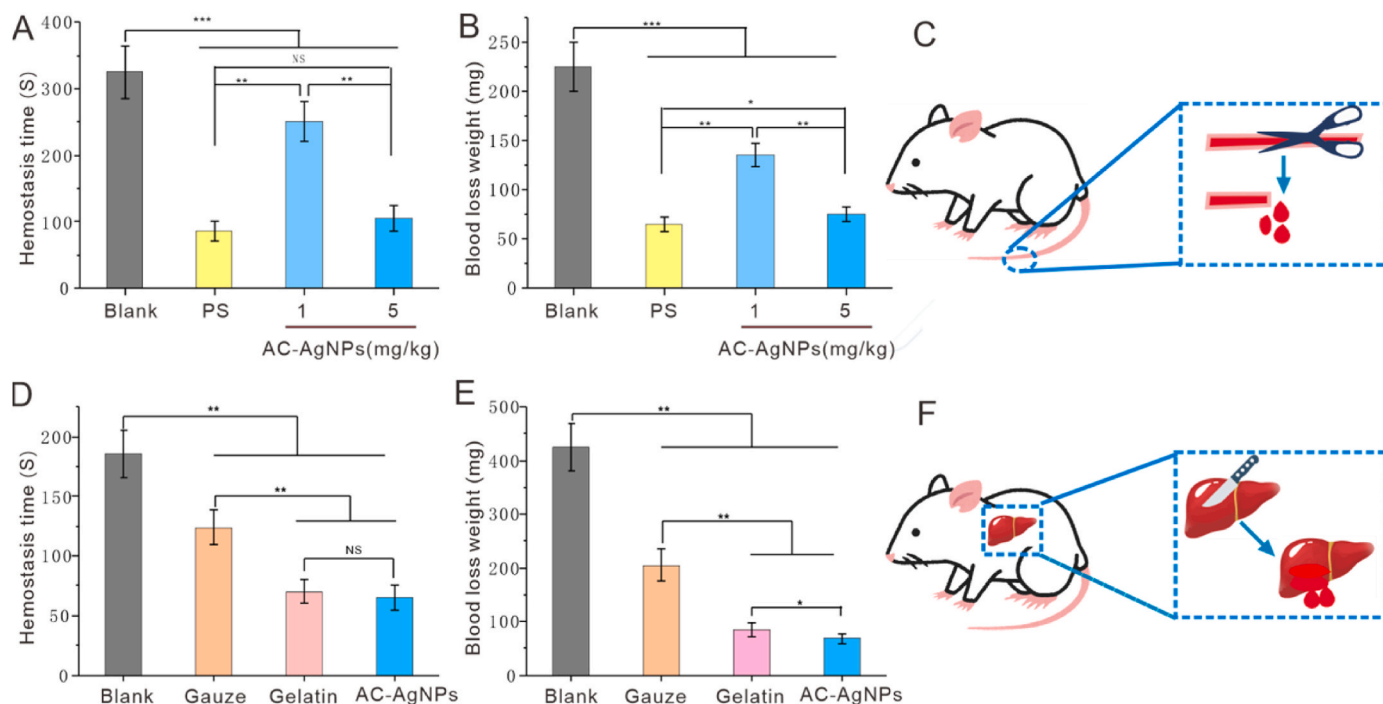


Fig. 6. In-vivo hemostatic capacity evaluation of AC-AgNPs. (A) hemostatic time and (B) blood loss in a mouse tail amputation model. The blank and protamine sulfate (PS) were negative and positive controls, respectively. (C) Schematic of the mouse tail amputation model. (D) hemostatic time and (E) blood loss in a mouse liver injury model. The blank, gauze, and gelatin were the control groups. (F) Schematic of the mouse liver injury model. * $P < 0.05$, ** $P < 0.01$, *** $P < 0.001$ using the Student's t-test (two-sided). The error bars stand for s.e.m. ($n = 5$).

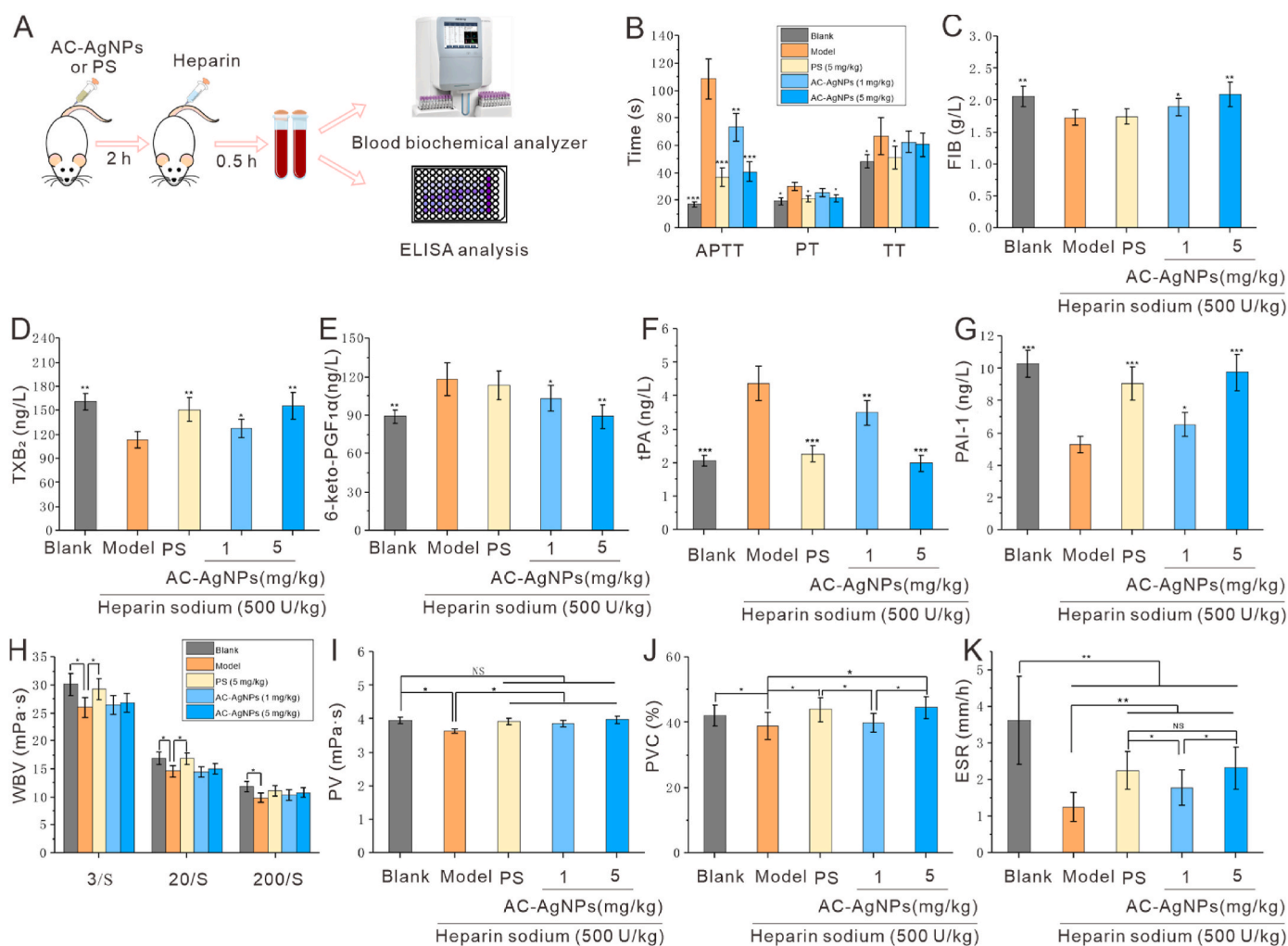


Fig. 7. Effect of AC-AgNPs on plasma coagulation parameters *in vivo*. (A) Schematic of related coagulation factor analysis. The related coagulation parameter analysis of (B) three main coagulation indices (APTT, PT, and TT), (C) FIB, (D) TXB₂, (E) 6-keto-PGF₁α, (F) tPA, (G) PAI-1, (H)WBV, (I) PV, (J) PVC, and (K) ESR after treatment with heparin, PS, and AC-AgNPs (−38 mV, 55 nm). Statistical significance was determined versus the model group (one-way ANOVA followed by a Student’s t-test). **P < 0.01, ***P < 0.001.

than in the control group. The AC-AgNPs group administered at a dosage of 5 mg/kg exhibited an increase in WBV, PV, PVC, and ESR, with effects comparable to the positive group, which revealed that AC-AgNPs influenced pro-coagulant impact by regulating the plasma viscosity.

All these results show that AC-AgNPs play a role in promoting blood coagulation.

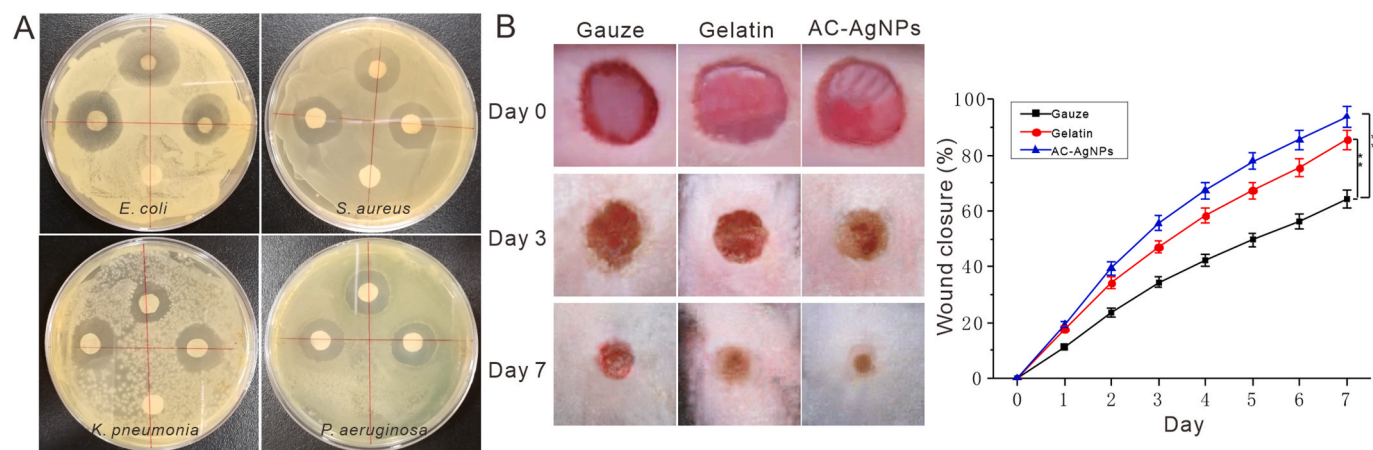


Fig. 8. *In-vivo* wound healing performance of AC-AgNPs. (A) Antibacterial effects of AC-AgNPs. (B) Wound contraction for Gauze, Gelatin, and AC-AgNPs. Compared with the Gauze group **P < 0.01 using Student’s t-test (two-sided). The error bar indicates the Standard Error (n = 5).

3.6. In-vivo wound healing and antibacterial performance of AC-AgNPs

It is well-documented that bacterial infection, local inflammation, and oxidative stress are the primary factors that contribute to delayed skin wound healing [47,48]. Our preliminary work has demonstrated that AC-AgNPs have strong antioxidant capacity both *in vitro* and *in vivo*. Here, we further investigated the antibacterial abilities of AC-AgNPs against *E. coli*, *K. pneumoniae*, *P. aeruginosa*, and *S. aureus*. As shown in Fig. 8A, Fig. S6, and Table S4, AC-AgNPs demonstrated remarkable antibacterial activity, and an increase in the size of the AC-AgNPs led to a decrease in the observed antibacterial effect. Obviously, dressings with antioxidant and antibacterial properties can prevent bacterial growth, alleviate inflammation, and lower the risk of infection, thereby facilitating proper wound healing. Thus, the wound healing performance of the AC-AgNP-embedded dressings was evaluated by an *in-vivo* test using a full-thickness skin defect model. As shown in Fig. 8B, all groups gradually reduced wound size as time progressed. Notably, the group treated with AC-AgNPs demonstrated a significantly higher closure rate than the gelatin and gauze groups. For instance, on the third day, the AC-AgNPs and gelatin groups exhibited an enhanced considerably wound contraction ratio compared to the gauze group ($P < 0.05$). By day 7, the wounds in the gauze group still had obvious scabbing with a closure rate of 64 %, whereas the AC-AgNPs group had almost completely recovered, achieving a closure rate of 93.69 %. All the results indicate that using AC-AgNPs can effectively reduce the risks of wound infection and expedite wound healing through the synergistic effect of phytoconstituents and the presence of AgNPs.

4. Conclusions

Pharmacologists have always attempted to synthesize and formulate new chemotherapeutic supplements or drugs using metallic nanoparticles derived from medicinal plants, based on their therapeutic properties [49,50]. In this study, we combined the antibacterial characteristics of AgNPs with the medicinal plant *A. conyzoides* to possess anti-inflammatory and hemostatic properties. Using an eco-friendly one-pot method, we produced AC-AgNP materials with controlled size

and surface charge, offering antibacterial, anti-inflammatory, and hemostatic functions. Then, we were systematically evaluated for their hemostatic effects and mechanisms of action (as illustrated in Fig. 9). *In vitro* coagulation performance experiments showed that AC-AgNPs have a strong hemostatic effect, which is related to their size, concentration, and negative charge. Cell experiment results show that AC-AgNPs have low cytotoxicity and hemolytic activity. Four-coagulation-test experiments shown that AC-AgNPs can shorten APTT and PT time, and increase FIB content, indicating its hemostatic pathway through intrinsic and extrinsic coagulation pathways. Western blot experiments exhibited that the negatively charged surfaces of AC-AgNPs can trigger a contact zymogen system by self-activation of Hageman factor FXII to promote the plasma KKS system. SEM and FCM experiments indicated that AC-AgNPs can induce platelet activation and aggregation, triggering the blood coagulation cascade. Furthermore, We conducted an in-depth network pharmacology analysis of the six chemical components encapsulated on the outer layer of AC-AgNPs. The results indicated that the target proteins of these compounds are mainly involved in the blood clotting cascade, the extrinsic pathway of fibrin clot formation, the complement system, and platelet activation and aggregation pathways. Subsequent molecular docking experiments also revealed that these six compounds interact with 13 core proteins related to coagulation and platelet activation to varying degrees. Among them, ameno flavone-7, 7^{'''}-dimethyl ether, 1,3,5-tricaffeoylquinic acid, and kaempferol 3,7, 4'-triglucoside may play a crucial role in these interactions. Additionally, *in-vivo* mouse tail amputation and mouse liver injury experiments showed that AC-AgNPs have better hemostatic and wound healing effects than gauze and gelatin. AC-AgNPs also increased the levels of thromboxane TXA2 and plasminogen activator inhibitor-1 PAI-1, while reducing the levels of prostacyclin PGI2 and tissue-type plasminogen activator tPA in the blood. Finally, wound healing experiments showed that AC-AgNPs effectively reduced the risk of infection and accelerated healing. It should be noted that this study has examined only the preliminary safety of AC-AgNPs in mice, we recognize the need to address the critical concern of embolism risk. Future research will comprehensively evaluate thrombotic risks through *in vivo* studies, dose-response analysis, drug interactions, biomarker monitoring, and risk-benefit

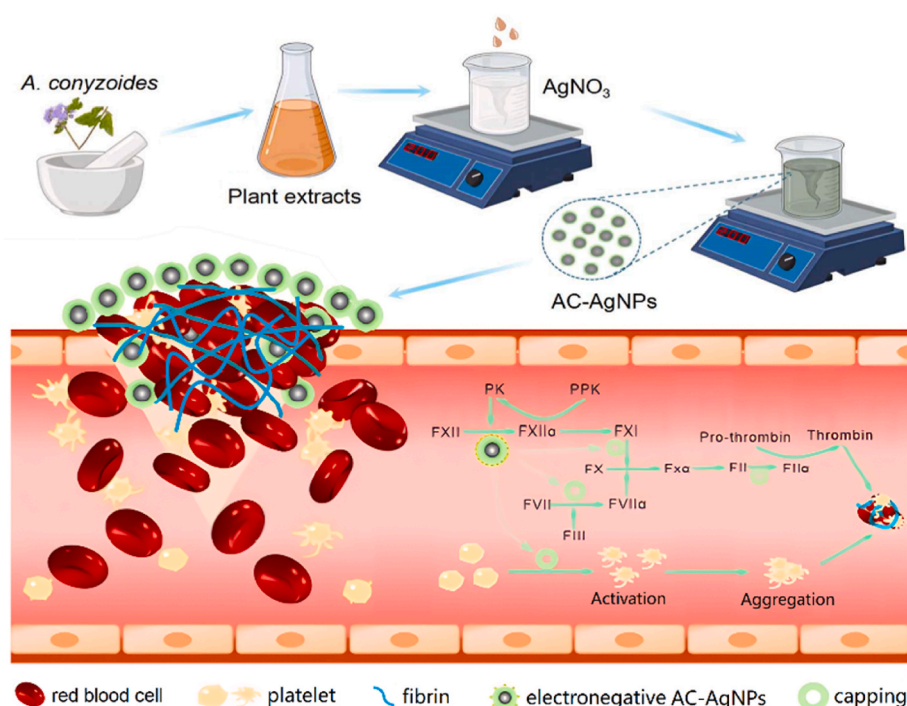


Fig. 9. Schematic illustration of AC-AgNPs hemostasis process.

assessments to ensure the safe clinical translation of AC-AgNPs. In summary, our research shows that green-synthesized AC-AgNPs may be a multifunctional hemostatic candidate material for practical applications.

CRedit authorship contribution statement

Yang Li: Methodology, Data curation. **Yinfeng Tan:** Software, Methodology, Data curation. **Huang Zhao:** Software, Methodology. **Shiting Chen:** Software. **Azadeh Nilghaz:** Writing – review & editing. **Rong Cao:** Writing – review & editing, Supervision, Funding acquisition. **Songlin Zhou:** Writing – original draft, Project administration, Methodology, Investigation, Funding acquisition, Data curation, Conceptualization.

Funding

This study was supported by the Hainan Provincial National Natural Science Foundation of China (Grant No. 522RC684), the Hainan Province Science and Technology Special Fund (Grant Nos. ZDYF2023SHFZ114, ZDYF2021SHFZ235), and the National Natural Science Foundation of China (Grant No. 82460757).

Declaration of competing interest

We state that there is no conflict of interest in submitting this manuscript and that all the authors have approved the manuscript for publication. On behalf of my co-authors, I would like to declare that the work described was original research that has not been published previously and is not under consideration for publication elsewhere, in whole or in part. All the authors listed have approved the manuscript that is enclosed.

Appendix A. Supplementary data

Supplementary data to this article can be found online at <https://doi.org/10.1016/j.mtbio.2025.101468>.

Data availability

Data will be made available on request.

References

- J.W. Cannon, Hemorrhagic shock, *N. Engl. J. Med.* 378 (4) (2018) 370–379.
- A. Uberoi, A. McCreedy-Vangi, E.A. Grice, The wound microbiota: microbial mechanisms of impaired wound healing and infection, *Nat. Rev. Microbiol.* 22 (8) (2024) 507–521.
- Y. Guo, M. Wang, Q. Liu, G. Liu, S. Wang, J. Li, Recent advances in the medical applications of hemostatic materials, *Theranostics* 13 (1) (2023) 161–196.
- M. Mecwan, J. Li, N. Falcone, M. Ermis, E. Torres, R. Morales, A. Hassani, R. Haghniaz, K. Mandal, S. Sharma, S. Maity, F. Zehtabi, B. Zamanian, R. Herculano, M. Akbari, V.J. J. A. Khademhosseini, Recent advances in biopolymer-based hemostatic materials, *Regen. Biomater.* 9 (2022) rbac063.
- J. Yang, T. Wang, L. Zhang, P. Fan, J. Zhao, X. Zheng, Y. Lai, H. Liu, S. Wang, Injectable hemostatic hydrogel adhesive with antioxidant, antibacterial and procoagulant properties for hemorrhage wound management, *J. Colloid Interface Sci.* 673 (2024) 395–410.
- A. Dehnooe, R.J. Kalbasi, M.M. Zangeneh, M.R. Delnavazi, A. Zangeneh, One-step synthesis of silver nanostructures using fruit extract, their cytotoxic activity, anti-cancer and anti-oxidant activities, *Micro & Nano Lett.* 18 (1) (2023) e12153.
- J.F. Bai, X. Gongsun, L.L. Xue, M.M. Zangeneh, Introducing a modern chemotherapeutic drug formulated by iron nanoparticles for the treatment of human lung cancer, *J. Exp. Nanosci.* 16 (1) (2021) 398–410.
- H.W. Zhao, H.T. Su, A. Ahmida, Y.Q. Sun, Z.Y. Li, M.M. Zangeneh, M. Nowrozi, A. Zangeneh, R. Moradi, Biosynthesis of copper nanoparticles using Boiss leaf aqueous extract; characterization and analysis of their antimicrobial and cutaneous wound-healing potentials, *Appl. Organomet. Chem.* 36 (12) (2022) e5587.
- P. Zhao, Y. Feng, Y. Zhou, C. Tan, M. Liu, Gold@Halloysite nanotubes-chitin composite hydrogel with antibacterial and hemostatic activity for wound healing, *Bioact. Mater.* 20 (2023) 355–367.
- Y. Wang, X. Nie, Z. Lv, Y. Hao, Q. Wang, Q. Wei, A fast hemostatic and enhanced photodynamic 2-dimensional metal-organic framework loaded aerogel patch for wound management, *J. Colloid Interface Sci.* 656 (2024) 376–388.
- W. Qiu, H. Han, M. Li, N. Li, Q. Wang, X. Qin, X. Wang, J. Yu, Y. Zhou, Y. Li, F. Li, D. Wu, Nanofibers reinforced injectable hydrogel with self-healing, antibacterial, and hemostatic properties for chronic wound healing, *J. Colloid Interface Sci.* 596 (2021) 312–323.
- T. Bruna, F. Maldonado-Bravo, P. Jara, N. Caro, Silver nanoparticles and their antibacterial applications, *Int. J. Mol. Sci.* 22 (13) (2021) 7202.
- E. Khadem, M. Kharaziha, S. Salehi, Colorimetric pH-responsive and hemostatic hydrogel-based bioadhesives containing functionalized silver nanoparticles, *Mater. Today Bio.* 20 (2023) 100650.
- W. Nie, X. Dai, D. Li, D. McCoul, G.J. Gillispie, Y. Zhang, B. Yu, C. He, One-Pot synthesis of silver nanoparticle incorporated mesoporous silica granules for hemorrhage control and antibacterial treatment, *ACS Biomater. Sci. Eng.* 4 (10) (2018) 3588–3599.
- S. Shakya, Y. He, X. Ren, T. Guo, A. Maharjan, T. Luo, T. Wang, R. Dhakhwa, B. Regmi, H. Li, R. Gref, J. Zhang, Ultrafine silver nanoparticles embedded in cyclodextrin metal-organic frameworks with GRGDS functionalization to promote antibacterial and wound healing application, *Small* 15 (27) (2019) e1901065.
- G. Wang, A. Ahmida, Z. Malek, S. Mansooridara, A. Zangeneh, M.M. Zangeneh, Chemical characterization and therapeutic properties of leaf aqueous extract synthesized copper nanoparticles against methamphetamine-induced cell death in PC12: a study in the nanotechnology and neurology fields, *Appl. Organomet. Chem.* 34 (4) (2020) e5488.
- L. Ma, A. Ahmida, K.F. Wang, A.R. Jalalvand, K. Sadrjavadi, M. Nowrozi, A. Zangeneh, M.M. Zangeneh, X.J. Wang, Introducing a novel chemotherapeutic drug formulated by iron nanoparticles for the clinical trial studies, *Appl. Organomet. Chem.* 36 (12) (2022) e5498.
- R. Dhir, S. Chauhan, P. Subham, S. Kumar, P. Sharma, A. Shidiki, G. Kumar, Plant-mediated synthesis of silver nanoparticles: unlocking their pharmacological potential—a comprehensive review, *Front. Bioeng. Biotechnol.* 11 (2023) 1324805.
- L.M. Zhang, L.F. Xu, Y. Wang, J.Y. Liu, G.H. Tan, F.Y. Huang, N.Y. He, Z.X. Lu, A novel therapeutic vaccine based on graphene oxide nanocomposite for tumor immunotherapy, *Chin. Chem. Lett.* 33 (8) (2022) 4089–4095.
- A. Ahmida, M.M. Zangeneh, A. Zangeneh, Green formulation and chemical characterization of Lens culinaris seed aqueous extract conjugated gold nanoparticles for the treatment of acute myeloid leukemia in comparison to mitoxantrone in a leukemic mouse model, *Appl. Organomet. Chem.* 34 (3) (2020) e5369.
- Y. Li, N. Li, W. Jiang, G.Y. Ma, M.M. Zangeneh, In situ decorated Au NPs on pectin-modified Fe₃O₄ NPs as a novel magnetic nanocomposite (Fe₃O₄/Pectin/Au) for catalytic reduction of nitroarenes and investigation of its anti-human lung cancer activities, *Int. J. Biol. Macromol.* 163 (2020) 2162–2171.
- N. Yadav, S.A. Ganie, B. Singh, A.K. Chhillar, S.S. Yadav, Phytochemical constituents and ethnopharmacological properties of *Ageratum conyzoides* L., *Phytother. Res.* 33 (9) (2019) 2163–2178.
- Z. Xu, X. Zha, R. Ji, H. Zhao, S. Zhou, Green biosynthesis of silver nanoparticles using aqueous extracts of *Ageratum conyzoides* and their anti-inflammatory effects, *ACS Appl. Mater. Interfaces* 15 (11) (2023) 13983–13992.
- M.B. Ponczek, A. Shamaev, A. LaPlace, S.K. Dickson, P. Srivastava, M.F. Sun, A. Gruber, C. Kastrup, J. Emsley, D. Gailani, The evolution of factor XI and the kallikrein-kinin system, *Blood Adv* 4 (24) (2020) 6135–6147.
- X. Gong, N.D. Jadhav, V.V. Lonikar, A.N. Kulkarni, H. Zhang, B.R. Sankpal, J. Ren, B.B. Xu, H.M. Pathan, Y. Ma, Z. Lin, E. Witherspoon, Z. Wang, Z. Guo, An overview of green synthesized silver nanoparticles towards bioactive antibacterial, antimicrobial and antifungal applications, *Adv. Colloid Interface Sci.* 323 (2024) 103053.
- J. Liu, A. Zangeneh, M.M. Zangeneh, B.H. Guo, Antioxidant, cytotoxicity, and anti-cancer properties of gold nanoparticles green synthesized by *Rhus coriaria* L. fruit aqueous extract, *J. Exp. Nanosci.* 15 (1) (2020) 202–216.
- A. Ahmida, A. Zangeneh, M.M. Zangeneh, Green synthesis and chemical characterization of gold nanoparticles synthesized using *Camellia sinensis* leaf aqueous extract for the treatment of acute myeloid leukemia in comparison to daunorubicin in a leukemic mouse model, *Appl. Organomet. Chem.* 34 (3) (2020) e5290.
- Z. Xu, R. Ji, X.R. Zha, H.G. Zhao, S.L. Zhou, The aqueous extracts inhibit inflammation by suppressing NLRP3 inflammasome activation, *J. Ethnopharmacol.* 309 (2023) 116353.
- X. Jin, Q. Ma, Z. Sun, X. Yang, Q. Zhou, G. Qu, Q. Liu, C. Liao, Z. Li, G. Jiang, Airborne fine particles induce hematological effects through regulating the crosstalk of the kallikrein-kinin, complement, and coagulation systems, *Environ. Sci. Technol.* 53 (5) (2019) 2840–2851.
- M. Tareq, Y.A. Khadrawy, M.M. Rageh, H.S. Mohammed, Dose-dependent biological toxicity of green synthesized silver nanoparticles in rat's brain, *Sci. Rep.* 12 (1) (2022) 22642.
- F. Hao, Q.S. Liu, X. Chen, X. Zhao, Q. Zhou, C. Liao, G. Jiang, Exploring the heterogeneity of nanoparticles in their interactions with plasma coagulation factor XII, *ACS Nano* 13 (2) (2019) 1990–2003.
- N. Mackman, H.M.H. Spronk, G.A. Stouffer, H. Ten Cate, Dual anticoagulant and antiplatelet therapy for coronary artery disease and peripheral artery disease patients, *Arterioscler. Thromb. Vasc. Biol.* 38 (4) (2018) 726–732.
- J. Shi, R. Tong, M. Zhou, Y. Gao, Y. Zhao, Y. Chen, W. Liu, G. Li, D. Lu, G. Meng, H. Hu, A. Yuan, X. Lu, J. Pu, Circadian nuclear receptor Rev-erb α is expressed by platelets and potentiates platelet activation and thrombus formation, *Eur. Heart J.* 43 (24) (2022) 2317–2334.

- [34] L. Baas, R. van der Graaf, E.S. van Hoorn, A.L. Bredenoord, K. Meijer, The ethics of gene therapy for hemophilia: a narrative review, *J. Thromb. Haemost.* 21 (3) (2023) 413–420.
- [35] M.V. Ragni, S.Y. Chan, Innovations in RNA therapy for hemophilia, *Blood* 142 (19) (2023) 1613–1621.
- [36] M. Sadaqat, M. Qasim, M. Tahir Ul Qamar, M.S. Masoud, U.A. Ashfaq, F. Noor, K. Fatima, K.S. Allemailem, F. Alrumaihi, A. Almatroudi, Advanced network pharmacology study reveals multi-pathway and multi-gene regulatory molecular mechanism of *Bacopa monnieri* in liver cancer based on data mining, molecular modeling, and microarray data analysis, *Comput. Biol. Med.* 161 (2023) 107059.
- [37] P. Minuz, A. Meneguzzi, L. Fumagalli, M. Degan, S. Calabria, R. Ferraro, M. Ricci, D. Veneri, G. Berton, Calcium-dependent Src phosphorylation and reactive oxygen species generation are implicated in the activation of human platelets induced by thromboxane A2 analogs, *Front. Pharmacol.* 9 (2018) 1081.
- [38] A. Opneja, S. Kapoor, E.X. Stavrou, Contribution of platelets, the coagulation and fibrinolytic systems to cutaneous wound healing, *Thromb. Res.* 179 (2019) 56–63.
- [39] D. Wang, P. Zhao, Y. Lv, J. Ming, Z. Wang, E. Yang, Y. Li, M. Wang, J. Niu, Y. Zhang, Y. Sun, Y. Chen, K. Chen, Z. Chen, W. Liu, X. Hu, Proteomic-based platelet activation-associated protein SELP may be a novel biomarker for coagulation and prognosis in essential thrombocythemia, *J. Clin. Med.* 12 (3) (2023) 1078.
- [40] X. Yi, J. Lin, H. Luo, C. Wang, Y. Liu, Genetic variants of PTGS2, TXA2R and TXAS1 are associated with carotid plaque vulnerability, platelet activation and TXA2 levels in ischemic stroke patients, *PLoS One* 12 (7) (2017) e0180704.
- [41] L.L. Yuan, X.Y. Jiang, M. Jiang, Y. Guo, Y.F. Liu, P.Y. Ming, S.L. Li, P.R. Zhou, R. Cai, K. Yu, G. Tao, Biocompatible gellan gum/sericin hydrogels containing halloysite@polydopamine nanotubes with hemostatic and photothermal antibacterial properties for promoting infectious wound repair, *Mater. Des.* 227 (2023) 111744.
- [42] X. Yang, Q. Wang, A. Zhang, X. Shao, T. Liu, B. Tang, G. Fang, Strategies for sustained release of heparin: a review, *Carbohydr. Polym.* 294 (2022) 119793.
- [43] J. Hogwood, B. Mulloy, E. Gray, Precipitation and neutralization of heparin from different sources by protamine sulfate, *Pharmaceuticals* 10 (3) (2017) 59.
- [44] L. Badimon, G. Vilahur, B. Rocca, C. Patrono, The key contribution of platelet and vascular arachidonic acid metabolism to the pathophysiology of atherothrombosis, *Cardiovasc. Res.* 117 (9) (2021) 2001–2015.
- [45] C.S. Whyte, H.A. Mostefai, K.M. Baeten, A.J. Lucking, D.E. Newby, N.J. Booth, M. N. Mutch, Role of shear stress and tPA concentration in the fibrinolytic potential of thrombi, *Int. J. Mol. Sci.* 22 (4) (2021) 2115.
- [46] X. Liu, J. Dong, Q. Liang, H.D. Wang, Z. Liu, R. Xu, W. Kang, Coagulant effects and mechanism of *Schefflera heptaphylla* (L.) Frodin, *Molecules* 24 (24) (2019) 4547.
- [47] Y. He, Y. Cen, M. Tian, Immunomodulatory hydrogels for skin wound healing: cellular targets and design strategy, *J. Mater. Chem. B* 12 (10) (2024) 2435–2458.
- [48] Y. Yang, J. Huang, A. Zeng, X. Long, N. Yu, X. Wang, The role of the skin microbiome in wound healing, *Burns Trauma* 12 (2024) tkad059.
- [49] A. Dehnoee, R.J. Kalbasi, M.M. Zangeneh, M.R. Delnavazi, A. Zangeneh, Characterization, anti-lung cancer activity, and cytotoxicity of bio-synthesized copper nanoparticles by *Thymus fedtschenkoi* leaf extract, *J. Clust. Sci.* 35 (3) (2024) 891–901.
- [50] M. Ishaq, P. Taslimi, Z. Shafiq, S. Khan, R.E. Salmas, M.M. Zangeneh, A. Saeed, A. Zangeneh, N. Sadeghian, A. Asari, H. Mohamad, Synthesis, bioactivity and binding energy calculations of novel 3-ethoxysalicylaldehyde based thiosemicarbazone derivatives, *Bioorg. Chem.* 100 (2020) 103924.